PCCP

PAPER

View Article Online
View Journal | View Issue

Cite this: *Phys. Chem. Chem. Phys.*, 2015, **17**, 15181

Functionalisation and immobilisation of an Au(110) surface *via* uracil and 2-thiouracil anchored layer

Oksana Plekan,*[a] Vitaliy Feyer,[b] Andrew Cassidy,[c] Victor Lyamayev,[d] Nataliya Tsud,[e] Sylwia Ptasińska,[f] Sara Reiff,[f] Rober G. Acres†[a] and Kevin C. Prince[ag]

Received 31st March 2015,
Accepted 2nd May 2015

DOI: 10.1039/c5cp01886b

www.rsc.org/pccp

We study surface functionalisation by uracil and 2-thiouracil, and immobilisation of several DNA moieties on functionalised gold surfaces. The combination of X-ray photoelectron and near-edge X-ray absorption spectroscopy allowed us to obtain a complete understanding of complex interfacial processes, starting from adsorption of biomolecules onto the metallic surface and progressing towards a specific surface functionality for interactions with other biologically related adsorbates. Au(110) surfaces were functionalised by deposition of uracil and 2-thiouracil molecules under vacuum conditions, and then tested for their selectivity by immobilisation of different DNA moieties deposited from aqueous solutions. We observed that adenine, adenosine, and RNA polymer (polyadenylic acid) from saturated solutions were immobilized successfully on the 2-thiouracil, but those from dilute (1%) solutions were not. However, cytosine failed to adsorb even from saturated solution. The chemical states of the biologically related adsorbates were investigated and the geometrical orientation of uracil and 2-thiouracil on the Au(110) surface was determined using both spectroscopic techniques.

Introduction

Functional layers of biomolecules on surfaces offer unique advantages in a variety of applications in the fields of biosensors, biomolecular diagnostics, and functionalized lab-in-chip devices. Functionalised surfaces play a vital role in biology and medicine, with the most essential biochemical reactions occurring preferably at the interfaces. Recent advances in surface science instrumentation have significantly increased our ability to better characterize surface compositions and molecular structures of biomaterials. These advances have greatly extended our capability to create novel biomaterials with well-predefined, desirable properties.[1,2] However, in order to achieve this goal, substantial research into the synthesis of individual molecules and the creation of complex molecular arrangements adsorbed on solid surfaces is still needed.

To understand the chemistry and structure of functionalised surfaces *via* biomolecules, it is important to obtain element-specific and bond-specific information at the interfaces. X-ray photoemission spectroscopy (XPS) and near-edge X-ray absorption fine structure spectroscopy (NEXAFS) are suitable techniques for this type of investigation. To date, we have studied the adsorption of a wide range of individual biomolecules on solid surfaces by employing both of these complementary spectroscopy methods.[3–12] In this work, we extended the scope of our research by increasing the size and complexity of the biological adsorbates. Two aspects of biometallic interfaces were addressed in this work. Firstly, we studied the functionalisation of a metal surface (Au(110)) with nucleobases, namely uracil and 2-thiouracil. The biolayers formed were characterized thoroughly using XPS and NEXAFS. Then, these biolayers, which acted as anchors, were probed for the immobilisation of complementary DNA moieties, following deposition from aqueous solutions.

Two nucleobases, uracil and 2-thiouracil (Fig. 1), were investigated here as anchoring layers on the Au(110) surface. In recent years, uracil derivatives have been used widely as building blocks to create functional nanostructures on surfaces by exploiting

[a] *Sincrotrone Trieste S.C.p.A., in Area Science Park, Strada Statale 14, km 163.5, I-34149 Basovizza, Trieste, Italy. E-mail: oksana.plekan@elettra.trieste.it; Fax: +39 0403758565; Tel: +39 0403758582*
[b] *Peter Grünberg Institute (PGI-6) and JARA-FIT, Research Center Jülich, 52425 Jülich, Germany*
[c] *Aarhus University, Department of Physics and Astronomy, Ny Munkegade 120, DK-8000 Aarhus C, Denmark*
[d] *European XFEL GmbH Albert-Einstein-Ring 19, 22761 Hamburg, Germany*
[e] *Charles University, Faculty of Mathematics and Physics, Department of Surface and Plasma Science, V Holešovičkách 2, 18000 Prague 8, Czech Republic*
[f] *Radiation Laboratory and Department of Physics, University of Notre Dame, Notre Dame, IN 46556, USA*
[g] *I.O.M.-C.N.R., in Area Science Park, Strada Statale 14, km 163.5, I-34149 Basovizza, Trieste, Italy*
† Present address: Australian Synchrotron, Imaging and Medical Beamline, 800 Blackburn Road, 3168, Clayton, VIC, Australia.

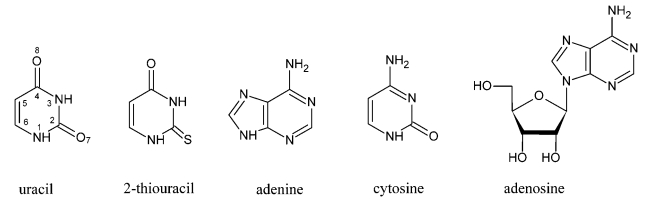

Fig. 1 Schematic structures of studied molecules.

molecular recognition.[13,14] There have been numerous scientific studies related to the adsorption of uracil on different surfaces, designed not only to understand the physical and chemical properties of specific systems, but also for potential applications in various domains of science and technology. Uracil was studied by scanning tunneling microscopy (STM) on MoS_2, where the molecules assembled into islands in which clearly distinguished dimers played an important role. However, the dimer motif is not found in the uracil single-crystal structure.[15,16] Vibrational spectroscopy studies have shown that uracil adsorbs on Si(100)-2×1 in its lactim form and bonds to the surface by cleavage of the O–H bond.[17] Many studies have characterised monolayers (ML) of uracil on metallic surfaces. On close-packed noble metal surfaces, STM, synchrotron XPS, and NEXAFS coupled with DFT (density functional theory) showed that uracil adsorbs almost flat on Ag(111).[18] The molecule remains intact and forms a densely packed hydrogen-bonded network with a poor long-range order.[18] Cyclic voltammetry experiments on Au(100),[19] Au(111),[20] and Ag(111)[21] have shown that the application of a potential at the electrode can switch the binding state from physi- to chemisorbed. DFT computational techniques have been employed to investigate chemisorbed uracil on Au(100) and Au(111) surfaces in order to describe the adsorption geometry on the substrate and to compare the core-level binding energies to those measured from similar systems (5-halouracils on Au(111),[11] and uracil chemisorbed on Cu(111)[18]).[22] It was found that on close-packed coinage metal surfaces, uracil chemisorbs more readily. As an example, on Cu(111), uracil deprotonated at the N3 site upon adsorption at room temperature.[18] Photoelectron diffraction, coupled with XPS and NEXAFS, indicated that for uracil adsorbed on Cu(110), N–H cleavage allows coordination to the surface through both O atoms, as well as the deprotonated N3 atom.[23] Moving beyond monolayers, the self-assembly of a uracil derivative, bis(uracil-ethynyl) benzene, on Ag(111) was discussed as a function of coverage and it was shown that upon increasing the molecular coverage, a disorder-to-order phase transition occurs.[24] Finally, NEXAFS of uracil at the C, N, and O K-edges was used to characterise the self-assembling molecular-stacking structure of the molecule.[25–27]

The gas phase photoemission spectrum of 2-thiouracil has been reported recently by Giuliano *et al.*[28] and we used these data here as a reference for the further interpretation of our spectra. In contrast to uracil, only a few studies have investigated the adsorption of 2-thiouracil on noble metal surfaces. In general, nucleobases adsorb very weakly on gold surfaces, whereas sulfur-containing molecules form strong stable bonds with Au, an interaction that is exploited primarily by a self-assembled monolayer (SAM) technique that involves alkanethiols.[29,30] Therefore, sulfur-substituted nucleobases, such as 2-thiouracil, can be anchored strongly on noble metal surfaces at monolayer coverage. Using surface X-ray diffraction, Meyerheim *et al.*[31] examined a monolayer of 2-thiouracil adsorbed on Ag(111). They found two different chemical states in which the molecular plane was tilted by either 31° or 36° with respect to the surface plane, and found that the C═S bond was lengthened by 0.17 Å, and that bond lengths within the pyrimidine ring also increased, all suggesting chemisorption. A Low Energy Electron Diffraction (LEED) study by Moritz *et al.*[32] confirmed these X-ray diffraction results and provided additional information, that the molecule bonds with the S atom in an essentially two-fold site: the Au–S bond length is 2.3 Å, and the distance between the molecule and the surface is 2.9 Å.

In this work, we compared uracil and 2-thiouracil and tested whether an Au(110) single crystal surface can be functionalised with a stable layer of these nucleobases. 2-Thiouracil was found to be anchored to the surface through an Au–S bond, while uracil remains physisorbed. Vacuum deposition was used to prepare the uracil or 2-thiouracil MLs and we observed that subsequent exposure to water increased the interaction between 2-thiouracil and Au, improving the stability of the anchoring layer. We then examined whether this functionalised surface was capable of immobilising other DNA moieties from aqueous solution, *i.e.*, whether the functionalised gold surface could detect the presence of complementary nucleobases. The RNA complementary base of uracil is adenine, therefore we investigated adenosine (purine nucleoside), and the non-complementary base cytosine to detect nucleobase partner recognition (see Fig. 1). All deposition steps for this immobilisation study were performed using aqueous solutions. Such liquid phase deposition is a ''soft'' method, because it is free from thermal decomposition, which may occur under UHV evaporation of such large molecules. Liquid phase deposition also takes us a step closer to possible ''real world'' applications.

Experimental

2.1. Experimental methods

The experiments were performed at the Materials Science Beamline at the Elettra synchrotron light source in Trieste.[33] The beamline is equipped with a plane grating monochromator providing synchrotron light in the energy range of ~22–1000 eV. The end station is equipped with a Specs Phoibos 150 hemispherical electron energy analyzer, LEED optics, and dual-anode X-ray source. The base pressure of the analysis chamber is $< 2 \times 10^{-10}$ mbar.

The Au(110) single crystal was cleaned *in situ* using standard procedures: cycles of Ar^+ sputtering, followed by annealing to 873 K. The surface order and cleanliness were monitored by LEED and XPS until contaminants (containing C, N, and O elements) were below the detection limits. The Au 4f core level spectra were recorded at a photon energy of 120 eV in normal emission geometry (incidence/emission angles of 60°/0°) and

the total resolution (analyser + beamline) was 0.15 eV. The C 1s and N 1s XPS data were collected in the same geometry, and the photon energy and total resolution were 500 eV and 0.45 eV, respectively. The O 1s core level spectra were measured at a photon energy of 630 eV with a total energy resolution of 0.85 eV. The binding energy (BE) was calibrated by measuring the Fermi edge for each photon energy. Valence band (VB) spectra measured at photon energy of 120 eV were used to check samples for radiation damage. No spectral changes were observed after 1 hour of exposure to radiation and we concluded that molecular films were stable under these experimental conditions.

NEXAFS was performed at the C, N, and O K-edges using the carbon, nitrogen, and oxygen KVV Auger yields (kinetic energy windows of 225–275, 355–390, and 495–525 eV, respectively) at normal incidence (NI, $\theta = 90^{\circ}$) and grazing incidence (GI, $\theta = 10^{\circ}$), where θ represents the angle between the propagation vector of the photon beam and the Au(110) surface plane. The gold crystal was mounted with its [001] crystallographic direction in the horizontal plane (perpendicular to the manipulator rotation axis). The manipulator allows for rotation in the azimuthal axis, and NEXAFS was also performed as a function of the angle between the photon beam polarization vector and the surface crystallographic orientations. The polarization of light from the beamline was not measured, but is expected to be between 80 and 90% linear, as the source is a bending magnet. The energy resolution in the C, N and O K-edge spectra was estimated to be 0.2, 0.35, and 0.6 eV, respectively. The raw NEXAFS and XPS data were normalized to the intensity of the photon beam, and measured by means of a high transmission gold mesh. In all cases, the corresponding spectra of the clean Au sample, recorded under identical conditions, were subtracted.

2.2. Sample preparation

Uracil and 2-thiouracil films were formed *in situ* by powder deposition in an adjoining sample preparation chamber (base pressure of 5×10^{-9} mbar), using a homemade Knudsen-cell type evaporator at temperatures of 373 K and 395 K, respectively. Prior to deposition, solid samples were degassed in vacuum at $\sim$350 K for several hours. Molecular films were dosed at a rate of $\sim$1.0 ML per min onto the clean Au surface. Monolayer coverage (saturated coverage) of 2-thiouracil was achieved by adsorbing multilayers of material on the surface and then flashing to 350 K to desorb weakly bound multilayers. This coverage was then defined as 1.0 ML and characterised by the integrated intensities (areas under peaks) of C 1s, N 1s, and O 1s measured *via* Mg Kα excitation. Uracil was not observed to form multilayers at the deposition temperature and only saturated monolayer coverage was observed.

For immobilisation studies, aqueous solutions of DNA moieties were deposited on the Au crystal under a nitrogen atmosphere in a glove bag connected to a fast entry lock of the chamber to avoid exposing of the crystal to ambient air. High purity water (18.2 MΩ cm from a MilliQ system) was used to prepare all aqueous solutions. Adenine, cytosine, adenosine, and polyadenylic acid, with the highest commercially available purities, were obtained from Sigma Aldrich and used without further purification. The saturation concentrations of adenine, cytosine, and adenosine in water at room temperature were 7.6, 65.8, and 19.2 mM, respectively.[34] Adenine and polyadenylic acid were deposited from saturated aqueous solutions. To ensure comparable molar concentrations, saturated solutions of cytosine and adenosine were prepared and then diluted to 9.4% and 37%, respectively. A 1% solution of adenine was prepared by diluting 1 ml of saturated adenine solution in 100 ml of high purity water. A drop of a prepared solution was placed on the Au crystal for 2 min and the crystal was then rinsed with high purity water and dried under nitrogen gas flow, after which it was transferred back into a vacuum for XPS and NEXAFS analyses.

Results

3.1 Anchored monolayers

Monolayers of uracil and 2-thiouracil were prepared on the Au(110) surface by vacuum deposition and in this section we discuss the characterisation of these monolayers using XPS and NEXAFS. Results pertaining to the exposure of the 2-thiouracil layer to water are also included so that the effects of the pure aqueous solution can be decoupled from the aqueous solutions used for the complementary nucleobase study presented in Section 3.2. Results for the uracil layer exposed to water are not presented as uracil forms a rather weak bond with Au(110) and can be easily washed out from the surface, leaving the clean Au surface.

Valence band spectra. Fig. 2(a) presents the valence band (VB) spectra for a clean gold surface (black, top) and surfaces with saturated coverage of uracil (red), 2-thiouracil (green), and 2-thiouracil after exposure to water (blue). Curves in Fig. 2(b) correspond to the VB spectra for the molecular films with the Au background subtracted, and curves in Fig. 2(c) show gas-phase molecular data for both biomolecules, taken at 100 eV photon energy. The gas-phase data have been shifted by -6.2 and -5.6 eV for uracil and 2-thiouracil, respectively, to obtain a better alignment of the main features with those in the solid state spectra of Fig. 2(b). These energy shifts were due to the work function of the samples (gas-phase spectra are referred to the vacuum level and solid state spectra to the Fermi level), plus relaxation shifts in the condensed state.

In Fig. 2(b), ten spectral features were identified in the BE range of 0–25 eV, and labeled (A–J) in the normalized valence band spectra for uracil, 2-thiouracil, and 2-thiouracil exposed to water. These assignments were performed based on the gas-phase experimental and theoretical data for uracil[35,36] and thiouracil.[37] According to these assignments, band B of 2-thiouracil corresponds to the ionization of the π_1 orbital and includes a contribution from the sulfur lone-pair (LP) (n_S). Features C and D in all three spectra represent four transitions and they were assigned to 5a″(π_5)/4a″(π_4) and 15a′(σ_O LP)/16a′(σ_O LP) orbitals from the pyrimidine aromatic ring and the C=O double bonds.[35] Band E was attributed to the 3a″(π_3) orbital.[39,40] At higher BEs, the spectra become more complex due to the overlapping structures formed by main peaks and satellites. In the BE range of $\sim$8–11 eV,

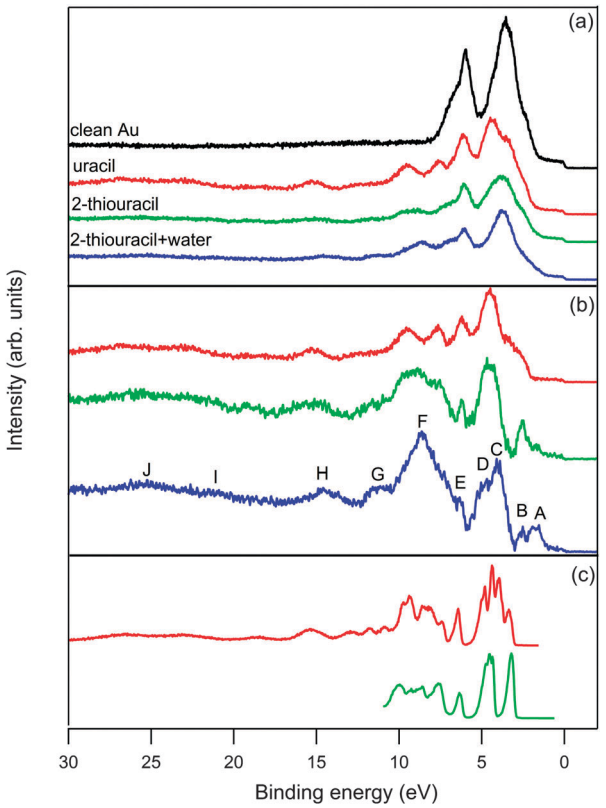

Fig. 2 (a) The valence band spectra measured with a photon energy of 120 eV for clean Au(110) surface (black); saturated coverage of uracil (red); saturated coverage of 2-thiouracil (green); and 2-thiouracil layer after exposure to water (blue); (b) Normalised spectra formed by subtraction of the clean Au(110) surface spectrum from the spectra for each molecular layer. (c) The gas phase valence band spectra for uracil and 2-thiouracil measured at photon energy of 100 eV.

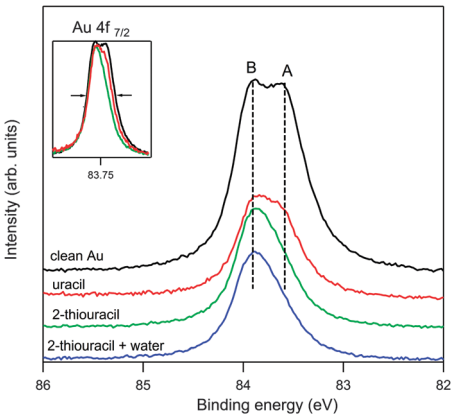

Fig. 3 Au $4f_{7/2}$ core-level spectra measured with a photon energy of 120 eV. From the top: (black) clean Au (110) surface; (red) uracil deposited in vacuum; (green) 2-thiouracil deposited in a vacuum; (blue) vacuum deposited 2-thiouracil after exposure to water. Inset: intensities of the clean surface spectra have been renormalized arbitrarily to allow comparison with other spectra in order to visualize the shift of the surface state A.

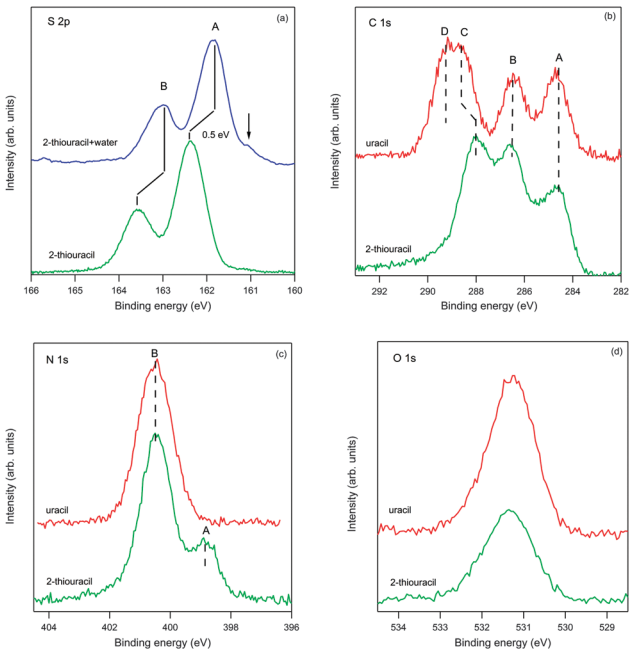

Fig. 4 (a) S 2p spectra from 2-thiouracil (green) and 2-thiouracil after exposure to water (top, blue). (b) C 1s, (c) N 1s and (d) O 1s spectra from uracil (red) and 2-thiouracil (green) measured at photon energies of 200 eV (S 2p), 500 eV (C 1s and N 1s) and 630 eV (O 1s) at NE geometry.

where the broad feature F is located, four main transitions appeared: $2a''(\pi_2)$, $14a'(\sigma)$, $13a'(\sigma_O)$, and $1a''(\pi_1)$. The peaks G–J at a higher BE range, from 11 to 26 eV, were due primarily to the ionisation of σ-bonding orbitals.[35]

The spectrum for 2-thiouracil exposed to water showed a new chemisorption state, band A, at a lower BE that was not observed for the pristine molecular film (Fig. 2(b)). This state is associated with the highest occupied molecular orbital (HOMO) of 2-thiouracil, which has a significant sulfur character.

Core level spectra. Au $4f_{7/2}$ core level spectra from the clean Au(110) surface, the surface upon adsorption of uracil and 2-thiouracil films deposited in a vacuum, and the 2-thiouracil film after exposure to water are presented in Fig. 3. The scans are offset in intensity for clarity. The clean Au(110) surface peak (top scan, Fig. 3) manifested a doublet structure assigned as A (83.64 eV) – the surface state and B (83.98 eV) – the bulk state.[38,39] While peak B did not exhibit a shift, peak A shifted by 50 meV upon adsorption of uracil, and 100 meV upon adsorption of 2-thiouracil, with respect to the clean surface. The attenuated signal and shift in peak A suggest a strong adsorbate–substrate interaction.

The core level spectra for S 2p, C 1s, N 1s, and O 1s recorded from saturated films of uracil and 2-thiouracil on the Au(110) surface are presented in Fig. 4. All spectra were fitted by Gaussian functions (not presented here) and the position of the peaks and assignments (based on the analysis of gas-phase spectra[28,40]) are summarized in Table 1. We compared the gas phase and surface-adsorbed spectra, as this provides insight into the interactions between the adsorbents and the Au(110) surface.

Two peaks, with binding energies of 162.38 and 163.58 eV (fits not shown), are visible in the S 2p spectra of the pristine 2-thiouracil layer on the Au(110) single crystal (Fig. 4(a)). These two peaks arise from the $2p_{3/2}$ and $2p_{1/2}$ doublet, and yielded a

Table 1 Position and assignment of the C, N and O 1s, and S 2p binding energies for uracil and 2-thiouracil molecules adsorbed on Au(110)

	Uracil on Au(110)	Uracil (gas phase)[40]	2-Thiouracil on Au(110)	2-Thiouracil (gas phase)[28]
C 1s	289.23 (D)/(C_2) 288.63 (C)/(C_4) 286.48 (B)/(C_6) 284.68 (A)/(C_5)	295.04 294.40 292.80 291.00	288.05 (C)/(C_2, C_4) 286.50 (B)/(C_6) 284.60 (A)/(C_5)	294.12 292.69 290.82
N 1s	400.48 (B)/(N_1, N_3)	406.80	400.45 (B)/(N_1, $N_{3,amino}$) 398.80 (A)/($N_{3,imino}$)	406.86
O 1s	531.25/(O_7, O_8)	537.60	531.35/(O_8)	537.36
S 2p			163.58(B) (S $p_{1/2}$) 162.38(A) (S $p_{3/2}$)	169.37 168.17

spin–orbit splitting of 1.2 eV and an intensity ratio of 2 : 1 between the $2p_{3/2}$ and $2p_{1/2}$ signals, as expected.[41] For 2-thiouracil films exposed to water (Fig. 4(a)), the S 2p peaks shifted by 0.5 eV to lower BE and a shoulder appeared at 161.0 eV.

The C 1s XPS results for uracil (Fig. 4(b)) have been decomposed into four components, with binding energies of 289.23, 288.63, 286.48, and 284.68 eV and these are assigned to C2, C4, C6, and C5 (for the labeling of the uracil molecule see Fig. 1). These assignments are in agreement with gas-phase data[40] and previous XPS data for uracil adsorbed on different metal surfaces.[18,42,43] For 2-thiouracil (Fig. 4(b)), the C 1s photoemission data correspond to the same 4 carbon atoms as for the uracil molecule (see Table 1).

The N 1s region in XPS of uracil (Fig. 4(c)) featured a single peak with a BE of 400.48 eV, which included two components that represent the two different N chemical environments, namely O═C_2–N_3–C_4═O and C_6–N_1–C_2═O. For 2-thiouracil (Fig. 4(c)), however, two well-resolved maxima, labelled A and B, were observed in the N 1s spectrum. As observed for uracil, there were two chemically distinct nitrogen atoms per 2-thiouracil molecule. The non-stoichiometric ratio between peaks A and B therefore implies that there are at least two chemically distinct molecular adsorption states present for the 2-thiouracil molecule on the Au surface. The oxygen photoemission data (Fig. 4(d)) for both uracil and 2-thiouracil displayed a single broad peak with a full width at half maximum of ∼1.45 eV and BE of ∼531.3 eV. This peak has been assigned to the carbonyl oxygen atoms O_7 and O_8 for uracil, and O_8 for 2-thiouracil (where the peak intensity is proportionally lower), see Table 1.

NEXAFS and molecular orientation. Polarization-dependent NEXAFS is an efficient tool to obtain information on the conformation and orientation of adsorbed molecules, as the intensities of the NEXAFS features depend on the photon incidence angle, θ, *i.e.*, the angle between the linear polarization of the light and the surface normal. For aromatic systems such as uracil and 2-thiouracil, the π^* states are derived from p_z orbitals oriented perpendicular to the molecular plane. If the aromatic π^* system lies parallel to the surface, the intensity of the corresponding transitions in the spectra exhibits a maximum for $\theta = 0°$ and vanishes for $\theta = 90°$.[44] The experimental N and O K-edge NEXAFS data of 1 ML of uracil, 2-thiouracil and 2-thiouracil exposed to water on Au(110) for normal incidence (NI, 90°), and grazing incidence (GI, 10°) photon beams are presented in Fig. 5 and 7. The spectra were taken using the *E*-vector of the incident photon beam aligned either perpendicular to the close-packed rows, *i.e.* in the Au [001] direction, or parallel (in the [1$\bar{1}$0] direction) at NI, and nearly normal to the surface ([110] direction) at GI (see Fig. 5(a) inset).

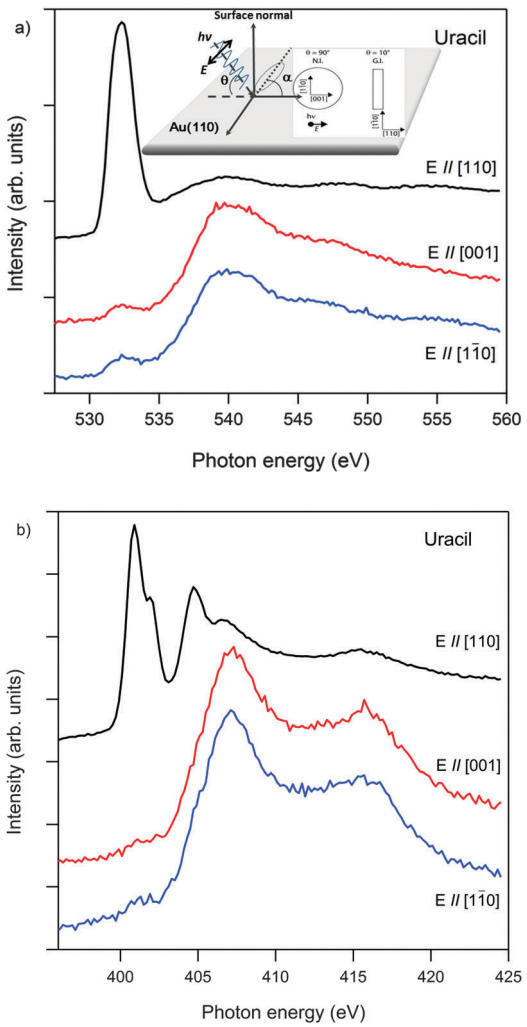

Fig. 5 (a) O K-edge and (b) N K-edge NEXAFS for uracil taken at GI (black) and taken at NI (red and blue).

The incidence angle θ between the *E*-vector of the linear polarized light and the surface normal was changed by rotating the sample with respect to the incoming beam. Hence, the C K-edge NEXAFS spectra were recorded at $\theta = 10^\circ$, 30°, and 50° (which is close to the "magic angle" for the given polarization ~90%, *i.e.*, the angle where the measured intensity distribution is independent of the molecular orientation), 70° and 90°. The intensities of the π* resonances as a function of photon incidence angle and polarization orientation are shown in Fig. 6 and 8. The positions and assignments for all individual peaks identified in all the NEXAFS spectra are compiled in Table 2.

The NEXAFS spectra at the N, O, and C K-edges can be divided into π*and σ* regions. The well-resolved, intense peaks in the low-photon energy range were assigned to transitions involving π* orbitals, while broad, less-intense features in the high-photon energy range were due to σ* orbitals. The assignments for all transitions (see Table 2) were based on available gas phase data for uracil[28] and experimental NEXAFS data for condensed uracil.[25–27] The dipole moment of the π* orbitals was oriented perpendicularly to the pyrimidine ring, and the stronger intensity of peaks involving π* transitions at grazing incidence (when $E_{\|}$[110], Fig. 5 and 6(a) and (b)) indicates that the ring was oriented essentially parallel to the Au(110) surface. The disappearance of the π* peak (relative to the σ* peaks) at normal incidence (when $E_{\|}[1\bar{1}0]$ or $E_{\|}$[001], Fig. 5(a) and (b) and bottom scan in Fig. 6(a) and (b)), in which the electric vector is parallel to the surface, is a sensitive measure of the geometrical orientation of the molecule on the surface. The angular resolution obtained in the C K-edge data allows the quantitative evolution of the adsorption geometry of uracil with respect to the Au surface (see Fig. 6(c)) because intensity depends on the angle between the incident E vector and the molecular orbital. In terms of quantitative analysis, the intensity of π* resonances ($I\pi^*$) at various incident angles (θ) can be expressed as follows:[44,45]

$$I\pi^* = CP(\sin^2\alpha\sin^2\theta + 2\cos^2\alpha\cos^2\theta) + C(1 - P)\sin^2\alpha, \quad (1)$$

where *C* is a normalization constant, *P* is the linear polarization factor (0.85), and α is the average tilt angle of π* vector orbital *versus* the surface normal (see Fig. 5(a) inset). Using the polarisation dependence to analyze the tilt angle of the π* orbital from the surface normal, we can conclude that uracil adsorbs flat onto the Au(110) surface (tilt angle to the surface plane $\alpha = 10^\circ \pm 5^\circ$), which is consistent with data in the literature.[25] The overall uncertainty of 5° takes into account fitting assumptions, fitting error, the degree of polarization of the X-ray beam, and the misalignment between the surface and reference manipulator orientation.

C 1s, N 1s, and O 1s NEXAFS data from 2-thiouracil films and 2-thiouracil films exposed to water are presented in Fig. 7 and 8. The oxygen and nitrogen K-edge spectra recorded for the as-deposited 2-thiouracil layer and the layer exposed to water resembled each other and there were no differences in the peak positions for both films (see Table 2). These spectra can be divided into π* (lower photon energy) and σ* (higher photon energy) regions. The excitation energies measured for the π* and σ* resonances are in agreement with previous data for uracil adsorbed on gold and the recently measured gas phase NEXAFS for 2-thiouracil.[28] The C 1s NEXAFS data (see Fig. 8) were dominated by three main bands arising from resonances associated with three carbon atoms, C_5, C_6, and C_4, of the pyrimidine ring.

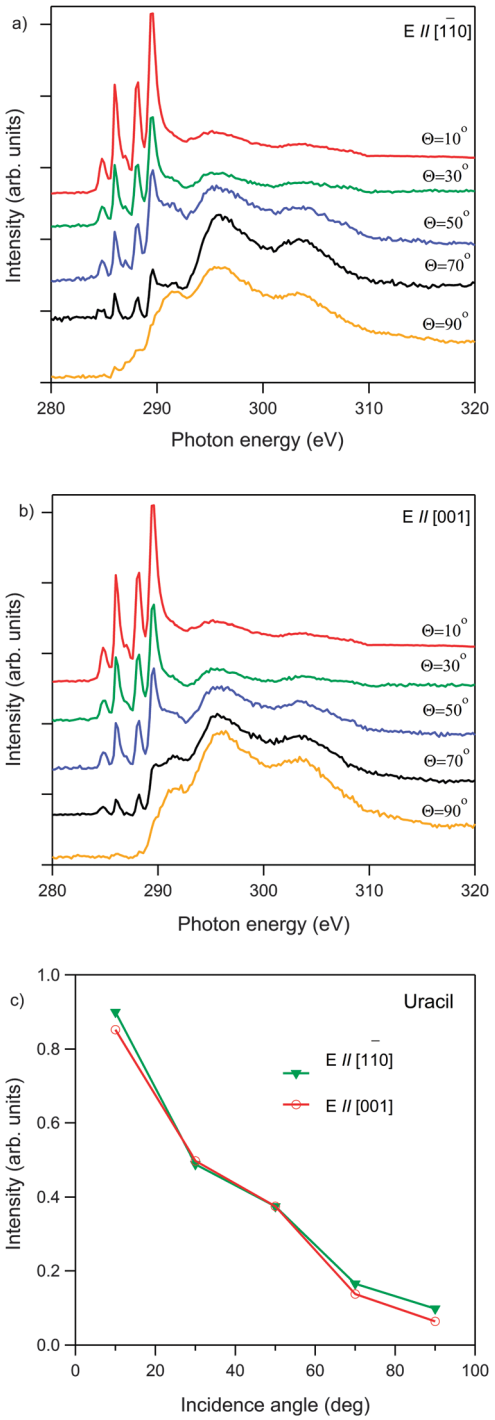

Fig. 6 C K-edge NEXAFS spectra of uracil recorded using the photon beam polarized parallel to (a) Au[1$\bar{1}$0] and (b) Au[001]. θ = the angle between the surface plane (Au(110)) and the propagation vector of the incident photon beam; starting from GI (10°) to NI (90°); (c) polarization dependence of the intensity of the π* resonances in the C 1s NEXAFS spectra of uracil.

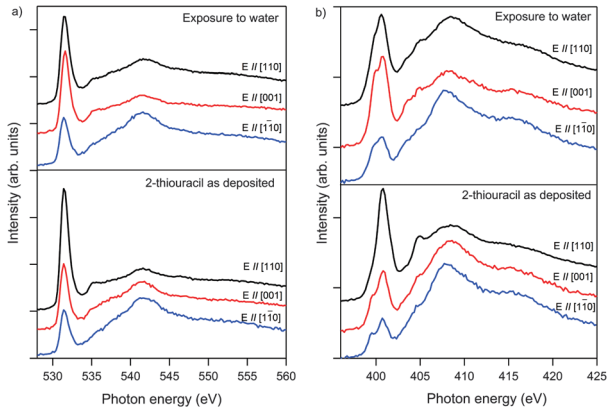

Fig. 7 (a) O K-edge and (b) N K-edge NEXAFS data for 1 ML 2-thiouracil exposed to water and 1 ML 2-thiouracil as deposited. Top scans (black) taken at GI and bottom two scans (red and blue) taken at NI.

The shoulder on the high energy side (~288.8 eV) can be compared to a similar feature in the NEXAFS spectrum of a 2-mercaptobenzoxazole multilayer on Pt(111).[46,47] Both 2-thiouracil and 2-mercaptobenzoxazole molecules contain C=S double bonds, and therefore, based on the theoretical and experimental results given in ref. 46 and 47, the peak at 288.8 eV can be assigned to the $C_2 \rightarrow \pi^*$ transition. The weak resonance at 290.6 eV resulted from to the C_6 1s $\rightarrow \pi^*$ and C_4 1s $\rightarrow \pi^*$ transitions. Applying the same eqn (1) to describe the angular dependence for the intensity of the C K-edge NEXAFS data in Fig. 8(c), the tilt angle between the 2-thiouracil molecular plane and the Au(110) surface was estimated to be $43^\circ \pm 5^\circ$ to the surface plane along the [001] direction, and $35^\circ \pm 5^\circ$ along the [1$\bar{1}$0] direction.

3.2 Immobilizing DNA moieties on the anchored 2-thiouracil monolayer

Having characterized the pristine molecular layers, we now describe the C and N 1s XPS data after exposing a monolayer of 2-thiouracil to different derivatives of complementary and non-complementary nucleobases. Note that only minor changes within the experimental resolution were observed in the O 1s and S 2p spectra; therefore, they are not discussed further. The immobilisation of adenine, cytosine, adenosine, and polyadenylic acid on uracil molecular monolayers was also attempted, but upon exposure to water, due to its rather weak bonding with Au(110), the uracil desorbed and only the clean Au surface remained.

Fig. 9 shows (a) the C 1s and (b) N 1s XPS spectra recorded after a monolayer of 2-thiouracil on Au(110) was exposed to aqueous solutions of adenine, cytosine, adenosine, and polyadenylic acid. In all cases, the vacuum-deposited 2-thiouracil monolayer on the Au(110) crystal, labelled as TU in Fig. 9, was exposed to water, labelled as TU + water. This TU + water layer was exposed subsequently to aqueous solutions containing one of the selected nucleobases or their derivatives. Table 3 compares the assignments of deconvoluted peaks and intensities of the C 1s and N 1s signals. The intensities of the total C and N signals were normalised to the pristine 2-thiouracil monolayer signal recorded after evaporation, *i.e.*, the C and N signals for the pristine ML samples

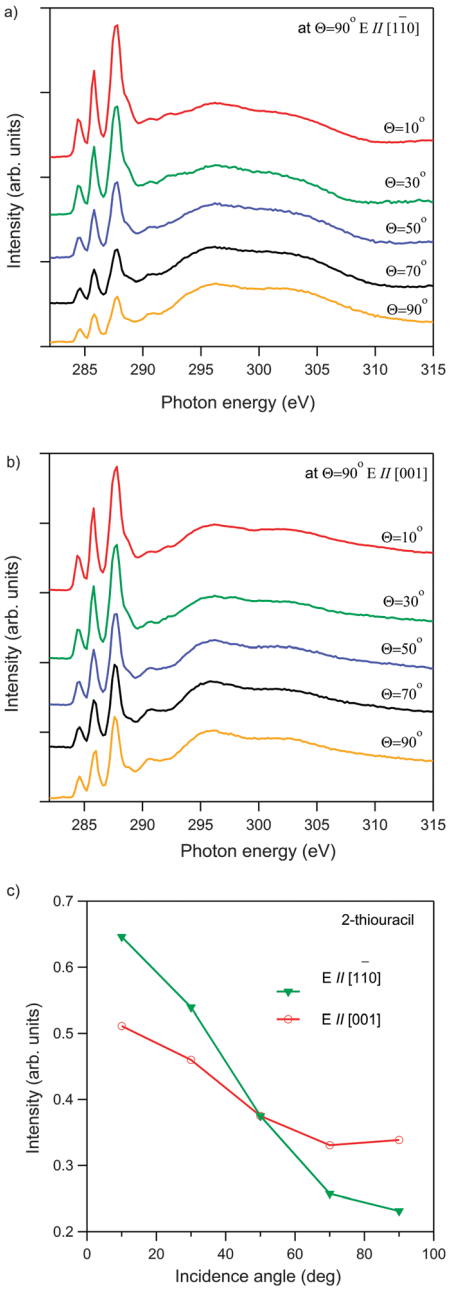

Fig. 8 C K-edge NEXAFS of 2-thiouracil as deposited, recorded with the photon beam polarized parallel to (a) Au[1$\bar{1}$0] and (b) [001]. θ = the angle between the surface plane (Au(110)) and the propagation vector of the incident photon beam; starting from GI(10°) to NI(90°); (c) polarization dependence of the intensity of the π^* resonances in the C 1s NEXAFS spectra of 2-thiouracil.

were normalized to 1 and an increase in the ratio shows that extra C or N was adsorbed on the surface after exposure. The absolute intensities (and hence the C and N normalised ratios) remained constant within the accuracy of the measurements for 1 ML of 2-thiouracil, TU + water, 1% adenine, and 9.4% cytosine. The C : N stoichiometric ratios were also preserved to within 4% (see Table 3). These data indicate that cytosine does not adsorb from a 9.4% solution and adenine does not adsorb from a 1% solution.

Table 2 Position and assignment of the individual peaks in the C, N and O 1s NEXAFS spectra of uracil and 2-thiouracil molecules

	Uracil	2-Thiouracil	2-Thiouracil exposed to water
C 1s	284.8/C_5 → LUMO ($\pi^*_{C=C}$)	284.4/C_5 → LUMO ($\pi^*_{C=C}$)	284.4/C_5 → LUMO ($\pi^*_{C=C}$)
	286.0/C_6 → LUMO ($\pi^*_{C=C}$)	285.8/C_6 → LUMO ($\pi^*_{C=C}$)	285.8/C_6 → LUMO ($\pi^*_{C=C}$)
	287.0/C_5 → π^* (shoulder)	287.8/C_4 → LUMO ($\pi^*_{C=O}$)	287.8/C_4 → LUMO ($\pi^*_{C=O}$)
	288.2/C_4 → LUMO ($\pi^*_{C=O}$)	288.8/C_2 → π^* (shoulder)	288.8/C_2 → π^* (shoulder)
	289.6/C_2 → LUMO ($\pi^*_{C=O}$)	290.6/$C_{4,6}$ → π^*	290.6/$C_{4,6}$ → π^*
	291.6/C_2 → π^* (shoulder)		
	296.0/(σ^*)	296.2/(σ^*)	296.2/(σ^*)
	303.6/(σ^*)	303.0/(σ^*)	303.0/(σ^*)
N 1s	400.9/$N_{1,3}$ → LUMO (π^*_{N-C})	399.4/$N_{1,3}$ → LUMO (π^*_{N-C})	400.0/$N_{1,3}$ → LUMO (π^*_{N-C})
	401.9/$N_{1,3}$ → LUMO (π^*_{N-C})	400.8/$N_{1,3}$ → LUMO (π^*_{N-C})	400.8/$N_{1,3}$ → LUMO (π^*_{N-C})
	404.7/$N_{1,3}$ → LUMO+1 (π^*_{N-C})	405.0/$N_{1,3}$ → LUMO+1 (π^*_{N-C})	405.0/$N_{1,3}$ → LUMO+1 (π^*_{N-C})
	407.1/($\sigma^*_{N-C=O}$)	408.2/($\sigma^*_{N-C=O}$)	408.6/($\sigma^*_{N-C=O}$)
	416.3/($\sigma^*_{N-C=O}$)	416.2/($\sigma^*_{N-C=O}$)	416.2/($\sigma^*_{N-C=O}$)
O 1s	532.3/$O_{7,8}$ → LUMO ($\pi^*_{O=C}$)	531.4/O_8 → LUMO ($\pi^*_{O=C}$)	531.4/O_8 → LUMO ($\pi^*_{O=C}$)
	540.3/($\sigma^*_{O=C}$)	535.2/($\sigma^*_{O=C}$)	535.2/($\sigma^*_{O=C}$)
	547.7/($\sigma^*_{O=C}$)	541.6/($\sigma^*_{O=C}$)	541.6/($\sigma^*_{O=C}$)

The C 1s XPS data in Fig. 9 showed differences in both peak position and intensity after a pristine ML was exposed to adenine, adenosine, and polyadenylic acid. The C 1s spectrum of the pristine 2-thiouracil monolayer showed three well-defined maxima at 284.6, 286.5, and 288.05 eV (see Table 3 and Fig. 4(b)). After exposure to water, these peaks were shifted towards lower BEs by 0.35 and 1.25 eV. In Fig. 9(a), dashed lines indicate the shifts to guide the eye. No changes were observed in either the C 1s or N 1s spectra following exposure of the TU + water to cytosine. The shape of C 1s spectra changed significantly for TU + water samples following deposition of adenine from saturated solution. The asymmetric and unresolved peak in the BE range from 288 to 285 eV is due to the additional carbon atoms that originated from the adenine moiety. The immobilisation of adenosine led to a strong peak centered at 286.68 eV, assigned to C–O–C and C–OH bonds mostly from the sugar ring.[8] After immobilisation of polyadenylic acid, the C 1s spectrum portrayed two new features: a very broad peak at 286.83, eV and a shoulder at 285.18 eV. Similar trends were also observed for the N 1s spectra (Fig. 9(b)).

After exposure to saturated solutions of DNA moieties: adenine, adenosine, or polyadenylic acid solutions, the TU + water sample showed changes in peak positions and intensity, strongly indicating that these nucleobases were immobilised on the surface through interaction with the 2-thiouracil monolayer. The ratio of imine to amine nitrogens increased following exposure to adenine, as was expected, as adenine ($C_5N_5H_5$) contains 3 imine- and 2 amine-nitrogen atoms. Immobilisation of adenosine ($C_{10}H_{13}N_5O_4$) led to further changes in the shape of the N 1s spectrum, appearance of a prominent peak at 399.03 eV and an unresolved shoulder at 400.18 eV. After adsorption of polyadenylic acid ($C_{30}H_{37}N_{15}O_{16}P_2$), the distinction between the amine and imine nitrogen peaks was lost and only one broad maximum centered at 399.33 eV was observed.

The effective thicknesses of the functionalised molecular layers on the Au(110) surface were estimated from the standard expression for the attenuation of the Au $4f_{7/2}$ photoelectron signal,

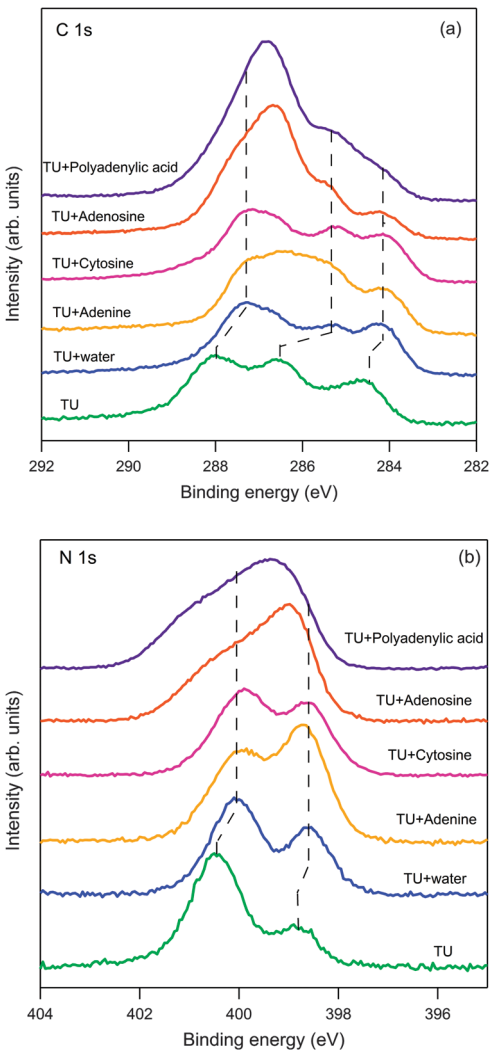

Fig. 9 (a) C 1s and (b) N 1s spectra of a pristine 2-thiouracil layer after adsorption (bottom), and after exposure to (from bottom to top) water, adenine (saturated), cytosine, adenosine and polyadenylic acid, in solution.

Table 3 C 1s and N 1s experimental binding energies for DNA moieties studied on functionalised Au(110)

Molecules	Core level	Assignments	Binding energy (eV)	Absolute area, counts/normalised ratio
TU (1 ML of vacuum deposited 2-thiouracil)	C 1s	C═S, C═O	288.05	405 856/1.00
		C–N	286.50	
		C–C	284.60	
	N 1s	N_1, N_3, amino	400.45	199 805/1.00
		N_3 imino	398.80	
TU + H_2O	C 1s	C═S, C═O	287.30	414 552/1.02
			286.70	
		C–N	(shoulder)	
		C–C	285.25	
			284.20	
	N 1s	N_1, N_3, amino	400.05	192 207/0.96
		N_3 imino	398.60	
TU + Adenine (saturated)	C 1s	C═S, C═O	287.20	471 595/1.16
		C–N	286.00	
		C–C	284.10	
	N 1s	N amino	399.95	262 215/1.31
		N imino	398.70	
TU + Adenine (1%)	C 1s	n/a	n/a	409 265/1.01
	N 1s	n/a	n/a	203 858/1.02
TU + Cytosine (9.4%)	C 1s	C═S, C═O	287.15	416 709/1.03
		C–N	286.20	
		C–C	284.05	
	N 1s	N amino	399.90	197 132/0.99
		N imino	398.60	
TU + Adenosine (37%)	C 1s	C═S, C═O	287.68 (shoulder)	513 843/1.27
		C–O–C	286.68	
		C–N, C–OH	285.43	
		C–C	284.13	
	N 1s	N amino	400.18	252 401/1.26
		N imino	399.03	
TU + Polyadenylic acid	C 1s	C═S, C═O, C–O–C	286.83	622 594/1.54
		C–N, C–OH, C–C	285.18	
	N 1s	N amino	400.78	273 801/1.37
		N imino	399.33	

recorded before and after deposition of biomolecules (see Fig. 3). A semi-quantitative estimation of the coverage of 2-thiouracil and uracil films was performed by using the Seah and Dench formula[48] for the parameterised inelastic mean free path for organic materials:

$$\lambda_m = 49 \Big/ E_k^2 + 0.11 \times \sqrt{E_k} \text{ mg m}^2 \quad (2)$$

where E_k is the kinetic energy of the emitted photoelectron. The values obtained were converted to length by dividing the known density for both compounds,[49,50] (1.50 g cm^{-3} for 2-thiouracil and 1.30 g cm^{-3} for uracil). Because the densities are similar, we expected to observe only small variations in the mean free path. The effective film thicknesses for 2-thiouracil and uracil (vacuum deposited) were calculated to be 3.4 and 3.5 Å, respectively. These numbers are comparable to the calculated size of the molecules,[31,50] and support the formation of a single layer of adsorbed molecules. The effective thickness is an index of how thick a layer is within a continuum model of the overlayer, and the number obtained is essentially qualitative as there is not enough structural information at the atomic level to quantify it more precisely.

Discussion

Vacuum deposition of 2-thiouracil onto the Au substrate at room temperature led to the development of a multilayered film, which, upon annealing to 350 K, left a stable monolayer coverage on the Au(110) surface. Multilayer desorption began at 325 K and the monolayer was not observed to desorb until 400 K. Multilayer deposition of uracil onto the same substrate was not possible at room temperature, indicating weaker intermolecular interactions with the Au(100) surface. Once stable monolayer coverage was achieved, the characterisation of the XPS core level and valence band data was made considerably easier through comparison with gas-phase data available in the literature. The electronic structures of the molecules in the gas phase are not perturbed by condensed-state effects (the surface work function, intermolecular forces, surface bonding interactions, *etc.*), and therefore, any differences between gas phase

and condensed phase spectra arise from interactions between the molecule and the Au surface. This was manifested predominantly by the peak broadening in the condensed phase data. The emergence of a new structure in the valence band, band A in Fig. 2(b), after exposure of the 2-thiouracil monolayer to water suggests a reconfiguration of the chemical bonding of the 2-thiouracil film. Peaks at such low binding energies are most likely related to the HOMO states, which for 2-thiouracil has a strong sulfur character, and the emergence of band A suggests that a new chemical bond was promoted between the S atom and the Au surface following exposure to water.[31] The sulfur–Au interaction is typically strong, and is exploited commonly in the fabrication of thiol-based self-assembled monolayers (SAMs). A similar effect, the emergence of a strong interaction following exposure to water, has also been discussed in relation to 5-bromouracil adsorbed on Au(111).[11]

Further evidence for a sulfur–Au covalent interaction was shown by the shift in the core level S 2p XPS data following exposure of 2-thiouracil to water (Fig. 4(a)). This shift was accompanied by the emergence of a shoulder at approximately 161.0 eV. Such a low BE peak has previously been attributed to sulfur present as a metal–sulfide complex.[51] Together, the BE shift and the appearance of the shoulder concur with the observation made above in relation to valence band data, namely the formation of a strong covalent bond between the 2-thiouracil sulfur atom and the Au(110) surface, accompanied by charge transfer from the gold substrate to this sulfur atom. This may be facilitated by a reconstruction of the gold surface.[52,53]

While both uracil and 2-thiouracil contain two N atoms (at positions 1 and 3 as described in Fig. 1), only one distinct peak was observed in the N 1s core level data for uracil, but two peaks were present in the 2-thiouracil spectrum Fig. 4(c). The higher BE peak, peak B at 400.45 eV, has been attributed to an amino state, while peak A at the lower BE of 398.80 eV is assigned to an imino chemical state. Peak A is therefore assumed to arise from the deprotonation of a single nitrogen atom on the 2-thiouracil molecule. This proton is not transferred intramolecularly, as evidenced by the absence of a change in the O 1s XPS data. Comparing the C 1s core level spectra for 2-thiouracil and uracil revealed that while peaks A and B (Fig. 4(b) bottom), assigned to C_5 and C_6 remained unaffected, peaks C (C_4) and D (C_2) both shifted to lower binding energies (by $\sim$1 eV) in the case of 2-thiouracil. This reflects the rearrangement of electron distribution after the deprotonation and allows us to identify N_3 as the deprotonation site. The intensity ratio between peaks A and B in the N 1s core level data in Fig. 4(c) was non-stoichiometric, indicating incomplete deprotonation. However, the ratio continued to change, observed as an increase of peak A after exposure to water (Fig. 9(b)). Here, deprotonation of the N atom was probably facilitated by bond reconfiguration, which takes place after the formation of the S–Au covalent bond, as discussed above. Deprotonation of the N_3 atom has previously been reported for uracil and other closely related species on a Cu(110) surface,[18,23] but in the gas phase, deprotonation does not occur and the N_1 atom is found to be the more acidic.[54] These observations lead to the conclusion that a fraction of the 2-thiouracil population is strongly attached to the Au substrate through an S–Au covalent bond and that the number of molecules attached increases after exposure to water. The absence of the S atom in the uracil molecule allows us to understand better why uracil did not bind strongly to the Au surface, and was washed away upon exposure to water.

Both the uracil and the 2-thiouracil molecules are planar and serve as excellent candidates for a NEXAFS study aimed at determining the geometric orientation relative to the substrate. The uracil molecule was found to lie almost flat on the Au surface (at an angle of $10^\circ \pm 5^\circ$) and consequently, there was no variation in the tilt angle with regard to the polarization vector of the incident photon beam. In contrast, there was a variation in the angular dependence of the C K-edge π^* transitions with regard to the angle between the photon beam polarization vector and the crystallographic orientation of the 2-thiouracil monolayer. This was expected, as the 2-thiouracil molecule lies at a significant angle on the Au surface, $43^\circ \pm 5^\circ$ in the [001] direction and $35^\circ \pm 5^\circ$ in the $[1\bar{1}0]$ direction. The geometric structure of an ordered monolayer of 2-thiouracil on Ag(111) was analysed previously using surface X-ray diffraction, and it was found that two different domains exist, with the pyrimidine rings tilted by either 31° or 36° with respect to the surface.[27] In a more recent work based on LEED results, Moritz *et al.*[32] proposed that the 2-thiouracil molecule lies tilted by 35° from the substrate plane. The results presented here, while measured on a different substrate, show that the angle between the molecule and the substrate is dependent on crystallographic orientation. The larger tilt angle of the 2-thiouracil molecule relative to the uracil molecule arises most likely from the geometrical adjustment required to facilitate the S–Au bond in the former.

In the DNA helix nucleobase complementarity is achieved through the formation of H-bonds between specific nucleobases. Non-complementary nucleobases cannot form these H-bonds and thus their interaction is much weaker. Cytosine is not the complementary base to 2-thiouracil (or uracil), and therefore, base–base interactions (crucial in determining the stability of the double helix) were not expected. Moreover, as confirmed by this study, cytosine was not immobilised on the 2-thiouracil covered surface, as shown in Table 3. All of the other DNA moieties: adenine, adenosine and polyadenylic acid, showed strong bonding to the 2-thiouracil anchoring layer and their adsorption was detected in the XPS data (Fig. 9).

Conclusions

The combination of C, N, and O 1s XPS data, together with NEXAFS data, have provided a clear picture of the adsorption structure of uracil and 2-thiouracil on the Au(110) surface. XPS data showed that 2-thiouracil chemisorbs on the Au surface *via* an Au–S bond and that the formation of this bond facilitates the deprotonation of the adjacent nitrogen atom and a restructuring of the surrounding carbon-bond network. We found that this new chemical state was particularly pronounced after the vacuum-deposited monolayer was exposed to water. NEXAFS was used to

determine the geometry of uracil and 2-thiouracil on the Au(110) surface, and the data showed that uracil lies flat on the surface, with a tilt angle of $10^\circ \pm 5^\circ$, while 2-thiouracil adopts a more upright orientation, with a tilt angle of $47^\circ \pm 5^\circ$ in the [001] direction, consistent with the formation of a covalent bond between the molecule and the gold surface. The tilt angle for 2-thiouracil was shown to depend on the orientation of the crystallographic axes and was $35^\circ \pm 5^\circ$ in the $[1\bar{1}0]$ direction.

2-Thiouracil molecules were also used as an anchoring layer to probe the interaction between complementary nucleobases. XPS was used to detect the immobilisation of complementary nucleobases on this 2-thiouracil monolayer. Adenine, adenosine, and polyadenylic acid were immobilised by the anchoring layer, while cytosine, a non-complementary base, was not immobilised, as expected.

Acknowledgements

The research leading to these results has received funding from the European Community's Seventh Framework Programme (FP7/2007–2013) under grant agreement No. 226716 and European Community FP7-ITN Marie-Curie Programme (LASSIE project, grant agreement #238258). S.P. and S.R. would like to thank the U.S. Department of Energy Office of Science, Office of Basic Energy Sciences under Award Number DE-FC02-04ER15533 for support and funds for S.R.'s travel to Elettra (NDRL No.:5063). The Materials Science Beamline is supported by the Ministry of Education of Czech Republic under Grant No. LG12003. We gratefully acknowledge the assistance of our colleagues at Elettra for providing good quality synchrotron light.

Notes and references

1 B. Kasemo, *Surf. Sci.*, 2002, **500**, 656.
2 D. G. Castner and B. D. Ratner, *Surf. Sci.*, 2002, **500**, 28.
3 O. Plekan, V. Feyer, F. Šutara, T. Skála, M. Svec, V. Cháb, V. Matolín and K. C. Prince, *Surf. Sci.*, 2007, **601**, 1973.
4 V. Feyer, O. Plekan, T. Skála, V. Cháb, V. Matolín and K. C. Prince, *J. Phys. Chem. B*, 2008, **112**, 13655.
5 V. Feyer, O. Plekan, K. C. Prince, F. Šutara, T. Skála, V. Cháb, V. Matolín, G. Stenuit and P. Umari, *Phys. Rev. B: Condens. Matter Mater. Phys.*, 2009, **79**, 155432.
6 V. Feyer, O. Plekan, N. Tsud, V. Matolín and K. C. Prince, *Langmuir*, 2010, **26**, 8606.
7 V. Feyer, O. Plekan, N. Tsud, V. Lyamayev, V. Cháb, V. Matolín, K. C. Prince and V. Carravetta, *J. Phys. Chem. C*, 2010, **114**, 10922.
8 O. Plekan, V. Feyer, S. Ptasińska, N. Tsud, V. Cháb, V. Matolín and K. C. Prince, *J. Phys. Chem. C*, 2010, **114**(1), 5036.
9 V. Feyer, O. Plekan, S. Ptasinska, M. Iakhnenko, N. Tsud and K. C. Prince, *J. Phys. Chem. C*, 2012, **116**, 22960.
10 V. Feyer, O. Plekan, F. Šutara, V. Cháb, V. Matolín and K. C. Prince, *Surf. Sci.*, 2011, **605**, 361.
11 O. Plekan, V. Feyer, N. Tsud, M. Vondráček, V. Cháb, V. Matolín and K. C. Prince, *Surf. Sci.*, 2012, **606**, 435.
12 O. Plekan, V. Feyer, S. Ptasińska, N. Tsud and K. C. Prince, *Phys. Chem. Chem. Phys.*, 2014, **216**, 6657.
13 T. Marangoni and D. Bonifazi, *Nanoscale*, 2013, **5**, 8837.
14 I. Radivojevic, I. Likhtina, X. Shi, S. Singh and C. M. Drain, *Chem. Commun.*, 2010, **46**, 1643.
15 S. J. Sowerby and G. B. Petersen, *J. Electroanal. Chem.*, 1997, **433**, 85.
16 J. S. Sowerby, M. Edelwirth and W. M. Heckl, *Appl. Phys. A: Mater. Sci. Process.*, 1998, **66**, S649.
17 A. Lopez, Q. Chen and N. V. Richardson, *Surf. Interface Anal.*, 2002, **33**, 441.
18 A. C. Papageorgiou, S. Fischer, J. Reichert, K. Diller, F. Blobner, F. Klappenberger, F. Allegretti, A. P. Seitsonen and J. V. Barth, *ACS Nano*, 2012, **6**, 2477.
19 Th. Dretschkow and Th. Wandlowski, *Electrochim. Acta*, 1998, **43**, 2991.
20 Th. Dretschkow, A. S. Dakkouri and T. h. Wandlowski, *Langmuir*, 1997, **13**, 2843.
21 M. Cavallini, G. Aloisi, M. Bracali and R. Guidelli, *J. Electroanal. Chem.*, 1998, **444**, 75.
22 S. Irrera, G. Portalone and N. H. De Leeuw, *Surf. Sci.*, 2013, **614**, 20.
23 D. A. Duncan, W. Unterberger, D. Kreikemeyer-Lorenzo and D. P. Woodruff, *J. Chem. Phys.*, 2011, **135**, 014704.
24 M. Enache, L. Maggini, A. Llanes-Pallas, T. A. Jung, D. Bonifazi and M. Stöhr, *J. Phys. Chem. C*, 2014, **118**, 15286.
25 K. Fujii, K. Akamatsu and A. Yokoya, *J. Phys. Chem. B*, 2004, **108**, 8031.
26 Y. Zubavichus, A. Shaporenko, V. Korolkov, M. Grunze and M. Zharnikov, *J. Phys. Chem. B*, 2008, **112**, 13711.
27 N. T. Samuel, C.-Y. Lee, L. J. Gamble, D. A. Fischer and D. G. Castner, *J. Electron Spectrosc. Relat. Phenom.*, 2006, **152**, 134.
28 B. M. Giuliano, V. Feyer, K. C. Prince, M. Coreno, L. Evangelisti, S. Melandri and W. Caminati, *J. Phys. Chem. A*, 2010, **114**, 12725.
29 A. Ulman, *Chem. Rev.*, 1996, **96**, 1533.
30 J. Ch. Love, L. A. Estroff, J. K. Kriebel, R. G. Nuzzo and G. M. Whitesides, *Chem. Rev.*, 2005, **105**, 1103.
31 H. L. Meyerheim, Th. Gloege and H. Maltor, *Surf. Sci.*, 1999, **442**, L1029.
32 W. Moritz, J. Landskron and M. Deschauer, *Surf. Sci.*, 2009, **603**, 1306.
33 R. Vašina, V. Kolařík, P. Doležel, M. Mynář, M. Vondráček, V. Cháb, J. Slezák, C. Comicioli and K. C. Prince, *Nucl. Instrum. Methods Phys. Res., Sect. A*, 2001, **467–468**, 561.
34 T. T. Herskovits and J. P. Harrington, *Biochemistry*, 1972, **11**, 4800.
35 D. M. P. Holland, A. W. Potts, L. Karlsson, I. L. Zaytseva, A. B. Trofimov and J. Schirmer, *Chem. Phys.*, 2008, **353**, 47.
36 O. Dolgounitcheva, V. G. Zakrzewski and J. V. Ortiz, *J. Phys. Chem. A*, 2002, **106**, 8411.
37 A. R. Katritzky, M. Szafran and G. Pfister-Guillouzo, *J. Chem. Soc., Perkin Trans. 2*, 1990, 871.
38 K. Heister, M. Zharnikov, M. Grunze and L. S. O. Johansson, *J. Phys. Chem. B*, 2001, **105**, 4058.

39 M. Iakhnenko, V. Feyer, N. Tsud, O. Plekan, F. Wang, M. Ahmed, O. Slobodyanyuk, R. G. Acres, V. Matolín and K. C. Prince, *J. Phys. Chem. C*, 2013, **117**, 18423.
40 V. Feyer, O. Plekan, R. Richter, M. Coreno, M. de Simone, K. C. Prince, A. B. Trofimov, I. L. Zaytseva and J. Schirmer, *J. Phys. Chem. A*, 2010, **114**, 10270.
41 M. Zharnikov and M. Grunze, *J. Phys.: Condens. Matter*, 2001, **13**, 11333.
42 A. Haug, S. Schweizer, F. Latteyer, M. B. Casu, H. Peisert, C. Ochsenfeld and T. Chasse, *ChemPhysChem*, 2008, **9**, 740.
43 J. Peeling, F. E. Hruska, D. M. McKinnon and M. S. Chauhan, *Can. J. Chem.*, 1978, **56**, 2405.
44 J. Stöhr, *NEXAFS Spectroscopy*, Springer-Verlag, Berlin, 1992.
45 K. Diller, F. Klappenberger, M. Marschall, K. Hermann, A. Nefedov, Ch. Wöll and J. V. Barth, *J. Chem. Phys.*, 2012, **136**, 014705.
46 V. Carravetta, G. Contini, O. Plashkevych, H. Ågren and G. Polzonetti, *J. Phys. Chem. A*, 1999, **103**, 4641.
47 G. Contini, V. Di Castro, S. Stranges, R. Richter and M. Alagia, *J. Phys. Chem. A*, 2000, **104**, 9675.
48 M. P. Seah and W. A. Dench, *Surf. Interface Anal.*, 1979, **1**, 2.
49 www.chemspider.com.
50 G. S Parry, *Acta Crystallogr.*, 1954, **7**, 313.
51 S. Berner, H. Lidbaum, G. Ledung, J. Åhlund, K. Nilson, J. Schiessling, U. Gelius, J.-E. Bäckvall, C. Puglia and S. Oscarsson, *Appl. Surf. Sci.*, 2007, **253**, 7540.
52 Y. Jeong, Ch. Lee, E. Ito, M. Hara and J. Noh, *Jpn. J. Appl. Phys.*, 2006, **45**, 5906.
53 K. Kummer, D. V. Vyalikh, G. Gavrila, A. Kade, M. Weigel-Jech, M. Mertig and S. L. Molodtsov, *J. Electron Spectrosc. Relat. Phenom.*, 2008, **163**, 59.
54 M. A. Kurinovich and J. K. Lee, *J. Am. Soc. Mass Spectrom.*, 2002, **13**, 985.

